Europhysics Letters PREPRINT

Multi-particle-collision dynamics: Flow around a circular and a square cylinder

A. LAMURA¹, G. GOMPPER¹, T. IHLE², and D. M. KROLL²

- ¹ Institut für Festkörperforschung, Forschungszentrum Jülich, D-52425 Jülich, Germany
- Supercomputing Institute, University of Minnesota,
 1200 Washington Ave. S., Minneapolis, MN 55415, USA

PACS. 02.70.Ns – Molecular dynamics and particle methods.

PACS. 47.11.+j – Computational methods in fluid dynamics.

PACS. 82.20.Wt - Computational modelling; simulation.

Abstract. – A particle-based model for mesoscopic fluid dynamics is used to simulate steady and unsteady flows around a circular and a square cylinder in a two-dimensional channel for a range of Reynolds number between 10 and 130. Numerical results for the recirculation length, the drag coefficient, and the Strouhal number are reported and compared with previous experimental measurements and computational fluid dynamics data. The good agreement demonstrates the potential of this method for the investigation of complex flows.

Introduction. – The simulation of the hydrodynamic behavior of complex fluids has attracted considerable attention in recent years. Several computational fluid dynamics approaches, such as lattice gas automata [1], lattice-Boltzmann methods [2, 3], and dissipative-particle dynamics [4], have been proposed and developed in order to describe the dynamical behavior of these systems on mesoscopic length scales. The first two methods, despite of their conceptual simplicity, suffer mainly from the lack of Galilean invariance. Moreover, since these are lattice based methods, practical applications involving irregular geometries often require the use of adapted computational meshes. Dissipative particle dynamics is an off-lattice, particle-based method which does not have these problems; however, it is often complex and difficult to analyze analytically.

In this Letter, we investigate in detail another particle-based simulation method which is a modification of Bird's Direct Simulation Monte Carlo algorithm [5]. The fluid is modeled by "particles" whose positions and velocities are continuous variables, while time is discretized. The system is coarse-grained into the cells of a regular lattice with no restriction on the number of particles per cell. The evolution of the system occurs in two steps: propagation and collision. Each particle is first streamed by its displacement during the time interval Δt . A novel algorithm for the collision step was introduced recently by Malevanets and Kapral [6]. The cells are the collision volumes for many-particle collisions — which is why we refer to this method as multi-particle collision dynamics (MPCD) —, which conserve mass, momentum and energy. In Ref. [6] it was shown that an H-theorem holds for this dynamics and that the

2 EUROPHYSICS LETTERS

correct hydrodynamic equations for an ideal gas are recovered. This model has been carefully studied in Ref. [7], where the Galilean invariance is critically discussed and it is shown that the original algorithm has to be modified at low temperatures to guarantee this symmetry.

We present the results of a quantitative analysis of the MPCD method in order to determine whether it can provide a convenient alternative to other computational fluid dynamics approaches. In particular, we study the problem of two-dimensional incompressible flow around a circular and a square cylinder. The available literature on this classical flow problem allows us to test and validate this new model.

After describing the method, we present computational results for a wide range of Reynolds number, covering both steady and unsteady periodic flows. The results are compared with previous experimental and numerical studies.

The model. – The system we study consists of N particles of unit mass with continuous positions $\mathbf{r}_i(t)$ and velocities $\mathbf{v}_i(t)$ in two dimensions, i = 1, 2, ..., N. The evolution is given by repeated streaming and collision steps. Assuming a unit time interval, $\Delta t = 1$, the particle positions change according to

$$\boldsymbol{r}_i(t+1) = \boldsymbol{r}_i(t) + \boldsymbol{v}_i(t) \tag{1}$$

during the streaming step. For the collision step, the system is divided into the cells of a regular lattice of mesh size a_0 , with $a_0 = 1$. Each of these cells is the collision volume for a multi-particle collision defined by

$$\mathbf{v}_i(t+1) = \mathbf{u}(t) + \Omega \left[\mathbf{v}_i(t) - \mathbf{u}(t) \right], \tag{2}$$

where u is the macroscopic velocity, defined as the average velocity of the colliding particles, which we assume to have coordinates of the center of the cell. Ω denotes a stochastic rotation matrix which rotates by an angle of either $+\pi/2$ or $-\pi/2$ with probability 1/2. The collisions are simultaneously performed on all the particles in a cell with the same rotation Ω , but Ω may differ from cell to cell. The local momentum and kinetic energy do not change under this dynamics.

The division of space into a fixed cell lattice for the collision step breaks Galilean invariance. This is a minor effect as long as the mean-free path is comparable or larger than the cell size a_0 , because subsequent collisions of a particle typically occur in different cells. On the other hand, when the mean-free path is small compared to the cell size a_0 , particles remain within the same cell for many collisions, and become correlated. These correlations depend on the presence of flow, and Galilean invariance is broken. It was shown in Ref. [7] that this problem can be cured by performing the collision operation in a cell grid which is shifted each time step by a random vector with components in the interval $[-a_0/2, a_0/2]$. The collision environment is then independent of the macroscopic velocity, and Galilean invariance is exactly restored.

No-slip boundary conditions. – For planar walls which coincide with the boundaries of the collision cells, no-slip boundary conditions are conveniently simulated in the case of a fixed cell lattice by employing a bounce-back rule, i.e. the velocities of particles which hit the wall are inverted after the collision. However, the walls will generally not coincide with, or even be parallel to, the cell boundaries. Furthermore, for small mean-free paths, when a shift operation of the cell lattice is required to guarantee Galilean invariance, partially occupied boundary cells are unavoidable, even in the simplest flow geometries.

We found that the simple bounce-back rule fails to guarantee no-slip boundary conditions in the case of partially filled cells. This can be demonstrated, for example, for a simple Poiseuille flow at low temperatures (small mean-free paths). The velocity profile for a channel of height H and length L (measured in units of the lattice constant) is shown in Fig. 1(a). The

Fig. 1 – Poiseuille flow through a channel of size $H=30a_0$ and $L=50a_0$, for $n_{av}=35$. (a) $k_BT=0.01275$, corresponding to a mean-free path $\ell=\Delta t(k_BT/m)^{1/2}=0.11$ (with $\Delta t=m=1$). The simulation is carried out with the shift operation of the collision cells. Results are shown for simple bounce-back boundary conditions (open circles) and for the boundary condition (3) (full circles). The dashed and solid lines are fits to a parabolic flow profile. (b) $k_BT=0.4$, corresponding to a mean-free path $\ell=0.63$. The simulation is carried out for a fixed cell lattice, which is displaced with respect to the walls by a quarter of the lattice constant, so that the cell lattice fills the channel asymmetrically.

velocity profile does not extrapolate to zero at the walls, and a strong slip is clearly visible. We therefore need a generalization of the bounce-back rule for partially filled cells. Many different schemes are possible. We propose the following algorithm, which we found both to be very efficient and to give good results — as discussed below. For all the cells of the channel which are cut by walls and therefore have a number of particles n smaller than the average number n_{av} of the bulk cells, we fill the 'wall' part of the cell with virtual particles in order to make the effective density of real plus virtual particles equal the average density. The velocities of the wall particles are drawn from a Maxwell-Boltzmann distribution of zero average velocity and the same temperature T as the fluid. The collision step, Eq. (2), is then carried out with the average velocity of all particles in the cell. Since the sum of random vectors drawn from a Gaussian distribution is again Gaussian-distributed, the velocities of the individual wall particles never have to be determined explicitly. Instead, the average velocity u in Eq. (2) can be written as

$$u = \frac{\sum_{i=1}^{n} v_i + a}{n_{av}} \tag{3}$$

where a is a vector whose components are numbers from a Maxwell-Boltzmann distribution with zero average and variance $(n_{av}-n)k_BT$ [8]. Results for Poiseuille flow with partially filled cells, both with cell-shifting and a fixed cell lattice, are shown in Fig. 1(a) and 1(b), respectively. The results are in very good agreement with the expected parabolic flow profile for kinematic viscosities $\nu=0.079\pm0.001$ and $\nu=0.087\pm0.001$, respectively, which should be compared with the values of $\nu=0.083\pm0.001$ and $\nu=0.088\pm0.001$ obtained from the (short-time) decay of the velocity autocorrelation function in an equilibrium system [7]. It is important to notice that the center-of-mass velocity of the virtual wall particles is non-zero in general, which reflects the non-zero temperature of the wall. Simulations of Poiseuille flow using the same boundary condition but with resting wall particles, i.e. $a\equiv0$ in Eq. (3), again fails to reproduce the desired flow profile. In this case, also the density of (real) particles increases drastically near the walls.

Fig. 2 – Velocity field at the final steady state for Re = 30 for the circular (left panel) and square (center panel) cylinder. Velocity field at Re = 100 for the square cylinder (right panel). Only a fraction of the simulation box is shown in each case.

Results and discussion. – The flow around a circular and a square cylinder with diameter D inside a plane channel of height H and length L was investigated. The blockage ratio B=D/H is fixed at 0.125 for both the cylinders. In order to reduce the influence of inflow and outflow boundary conditions, the length L is set to L/D=50. The cylinder is centered inside the channel at a distance L/4 from the inflow region. The average number of particles per cell is $n_{av}=10$ and the temperature is fixed at $k_BT=0.4$; the corresponding viscosity is $\nu=0.110\pm0.004$. The flow is driven by assigning Maxwell-Boltzmann-distributed velocities

4 EUROPHYSICS LETTERS

with parabolic profile $v_x(y) = 4v_{max}(H-y)y/H^2$ to particles in the region $0 < x \le 10$. The maximum flow velocity, v_{max} , is fixed by the condition that the Mach number — i.e. the velocity relative to the speed of sound c, with $c^2 = [C_p/C_v]dp/d\rho = 2k_BT/m$ — is approximately 1/4, in order to avoid significant compressibility effects. Periodic boundary conditions are imposed in the x-direction, no-slip boundary conditions on the channel and cylinder walls.

Reynolds numbers, $Re \equiv v_{max}D/\nu$, in the range $10 \le Re \le 130$ were investigated. Both steady flows, with a closed steady recirculation region consisting of two symmetric vortices behind the body, and unsteady flows, with the well-known von Karman vortex street with periodic vortex shedding from the cylinder, are observed to occur for this range of Reynolds numbers. The critical Reynolds number above which flow becomes unsteady, is approximately 49 for the circular cylinder [9] and 60 for the square cylinder [10]. Figure 2 shows the macroscopic velocity field of the final steady-state for Re = 30, and of the periodic vortex shedding for Re = 100.

Fig. 3 – The recirculation length as a function of the Reynolds number. Square cylinder: (\bullet) this study with fixed cell lattice, (\circ) this study with cell-shifting, (——) Breuer *et al.* [10]; Circular cylinder: (\star) this study with fixed cell lattice, (\triangle) this study with cell-shifting, (— —) Coutanceau and Bouard [11].

Fig. 4 – The drag coefficient $C_d = 2F_{\parallel}/(n_{av}v_{max}^2D)$ — where F_{\parallel} is the force exerted on the cylinder in the direction parallel to the flow — as a function of the Reynolds number. Square cylinder: (•) this study, (——) Breuer *et al.* [10]; Circular cylinder: (*) this study, (o) Tritton [12], (\triangle) He and Doolen [13].

Such flow patterns are consistent with experiments (cfr. Fig. 4 of Ref. [11] for the circular cylinder) and simulations (cfr. Fig. 2 of Ref. [10] for the square cylinder). The length, L_r , of the recirculation region, from the rear-most point of the cylinder to the end of the wake, has been measured in units of D. Results, with error bars, are shown in Fig. 3 for both the square and circular cylinders. The errors are estimated to be 1/(2D), since the position of the macroscopic velocity u in each cell is arbitrarily taken to be the center of the cell. Our results for L_r/D are consistent with a linear increase with Reynolds number. Our data for the circular cylinder compare very well with experimental measurements for a similar value of the blockage ratio (B = 0.12) [11]. Indeed, L_r/D is a sensitive function on B, and increases with decreasing B [11]. No numerical data are available for a similar value of B. In the case of the square cylinder, our data can be compared with the numerical results of Ref. [10], obtained using lattice-Boltzmann and finite-volume methods with the same blockage ratio B = 0.125 and same parabolic inflow velocity profile as in our study. A linear fit to our data obtained both with cell-shifting as well as the fixed-cell lattice data for Re = 10 gives

$$L_r/D = -a + b \cdot Re \tag{4}$$

with $a=0.148\pm0.069$ and $b=0.0525\pm0.0020$ while Breuer et al. find a=0.065 and b=0.0554. The slopes are very similar, but our data are shifted to somewhat smaller values of L_r/D . For the square cylinder, no experimental data could be found in the literature.

Figure 4 shows the drag coefficient C_d as a function of the Reynolds number. For the square cylinder, agreement between our data and the previous numerical measurements is satisfactory, with a small but systematic deviation to larger values compared to Ref. [10] for Re > 20. In the case of the circular cylinder, our results are compared with the experimental measurements of Tritton [12], and with numerical simulations by He and Doolen [13] performed

with a lattice-Boltzmann method implemented on a variable mesh. In contrast to the current simulations, Refs. [12] and [13] both used a constant incoming velocity profile and a very small blockage ratio.

Our results fall below (about 5%) the literature data in this case. This is mainly due to the different boundary conditions and blockage ratios used in the various studies. Numerical investigations with the lattice-Boltzmann method [14] showed that C_d depends on the profile of the incoming flow. In Ref. [13], lateral periodic boundaries and a constant inflow velocity profile instead of no-slip boundary conditions with a parabolic inflow velocity profile were used. It was shown in Ref. [14] that $C_d(no-slip)/C_d(periodic)=0.82$ for B=0.1 (no error bar given). It seems reasonable to expect a similar behavior also for the present case. Indeed, the comparison of our results with those of the lattice-Boltzmann simulation [14] gives a ratio of $C_d(no-slip)/C_d(periodic)=0.90\pm0.03$.

Fig. 5 – The Strouhal number as a function of the Reynolds number. Square cylinder: (\bullet) this study, (\diamond) Breuer *et al.* [10]; Circular cylinder: (\star) this study, (\diamond) Tritton [12], (\triangle) He and Doolen [13], (\star) Williamson [15]. Both lines are guides to the eye.

In the unsteady flow regime we computed the lift coefficient $C_l = 2F_{\perp}/(n_{av}v_{max}^2D)$, where F_{\perp} is the force excerted on the cylinder in the direction perpendicular to the flow. The characteristic frequency f of the vortex shedding was determined by a spectral analysis (fast Fourier transform) of the time series of C_l and used to determine the Strouhal number $St \equiv fD/v_{max}$ [8]. Our data as a function of Re are shown in Fig. 5. They lie within the range of scatter of the published data. We want to mention again that for the circular cylinder, the existing literature were all obtained using different inflow conditions than in our study.

Conclusions. – The multi-particle collision dynamics method has been successfully applied to simulate two-dimensional flow around a circular and a square cylinder. The results are found to be in good agreement with previous experimental measurements and computational fluid dynamics studies. The computational efficiency of the MPCD method can be estimated from the time requirement of about 1.7 seconds (1.2 seconds) per time step for a system of 2 million particles with (without) cell-shifting on a Compaq XP1000 (667 MHz) workstation.

The main difference between multi-particle collision dynamics and lattice Boltzmann and finite-volume methods, which have been employed in most other studies of this flow geometry, is the presence of thermal fluctuations. In equilibrium, these fluctuations are responsible for a logarithmic divergence of the viscosity with time [7, 16], a divergence which is cut off by the finite system size at long times. A thermal renormalization of the viscosity could indeed be responsible for the small deviations of the values for the recirculation length and the drag coefficient compared to the lattice Boltzmann results.

The present model provides a simple alternative scheme that can be used to treat a wide class of physical and chemical problems. Many directions are accessible to exploration. The results presented here are relevant for studies of the interactions among large colloidal particles in solution. The algorithm can also be used for a mesoscopic model of the solvent dynamics which can be coupled to a microscopic treatment of solute particles.

* * *

A.L. thanks the Supercomputing Institute of the University of Minnesota for its hospitality. Support from the National Science Foundation under Grant Nos. DMR-9712134 and DMR-0083219, and the donors of the Petroleum Research Fund, administered by the ACS, are

6 EUROPHYSICS LETTERS

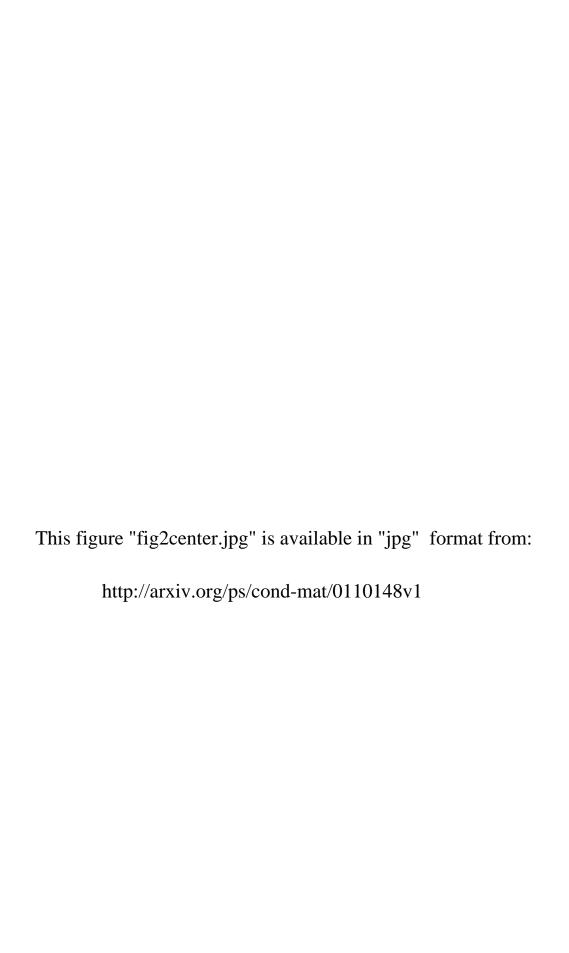
gratefully acknowledged.

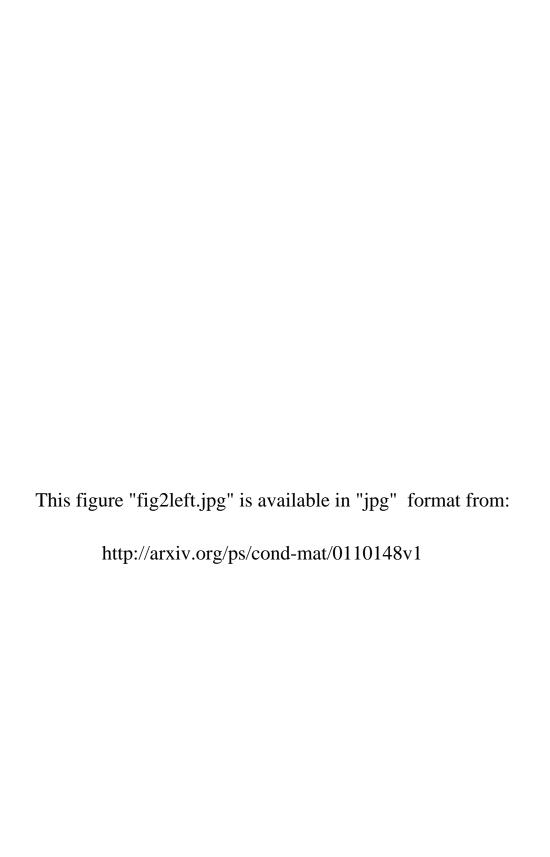
REFERENCES

- [1] Frisch U., Hasslacher B. and Pomeau Y., Phys. Rev. Lett., 56 (1986) 1505.
- [2] McNamara G. R. and Zanetti G., Phys. Rev. Lett., 61 (1988) 2332.
- [3] HIGUERA F. J. and JIMENEZ J., Europhys. Lett., 9 (1989) 663.
- [4] PAGONABARRAGA I., HAGEN M. H. J. and FRENKEL D., Europhys. Lett., 42 (1998) 377.
- [5] Bird G. A., Molecular Gas Dynamics (Clarendon Press, Oxford) 1976.
- [6] Malevanets A. and Kapral R., J. Chem. Phys., 110 (1999) 8505; ibid., 112 (2000) 7269.
- [7] IHLE T. and KROLL D. M., Phys. Rev. E, 63 (2001) 020201(R).
- [8] Details will appear elsewhere.
- [9] WILLIAMSON C. H. K., Annu. Rev. Fluid Mech., 23 (1996) 477.
- [10] Breuer M., Bernsdorf J., Zeiser T. and Durst F., Int. J. Heat Fluid Flow, 21 (2000) 186.
- [11] COUTANCEAU M. and BOUARD R., J. Fluid Mech., 79 (1977) 231.
- [12] TRITTON D. J., J. Fluid Mech., 6 (1959) 547.
- [13] HE H. and DOOLEN G., J. Comput. Phys., 134 (1997) 306; Phys. Rev. E, 56 (1997) 434.
- [14] Wagner L., Phys. Rev. E, 49 (1994) 2115.
- [15] WILLIAMSON C. H. K., Phys. Fluids, **31** (1988) 2742.
- [16] Ernst M. H., Hauge E. H., and van Leeuwen J. M. J., Phys. Rev. Lett., 25 (1970) 1254.

This figure "fig1a.jpg" is available in "jpg" format from:

This figure "fig1b.jpg" is available in "jpg" format from:





This figure "fig2right.jpg" is available in "jpg" format from: http://arxiv.org/ps/cond-mat/0110148v1

This figure "fig3.jpg" is available in "jpg" format from:

This figure "fig4.jpg" is available in "jpg" format from:

This figure "fig5.jpg" is available in "jpg" format from: